Mon. Not. R. Astron. Soc. **666**, 1–10 (1999) Printed 24 June 1999 (MN LATEX style file v1.4)

Quantifying the evolution of higher–order clustering

Jens Schmalzing[1,2,⋆], Stefan Gottlöber[3,4,†], Anatoly A. Klypin[4,‡], and Andrey V. Kravtsov[4,§]

[1] *Max–Planck–Institut für Astrophysik, Karl–Schwarzschild–Straße 1, 85740 Garching, Germany.*
[2] *Ludwig–Maximilians–Universität, Theresienstraße 37, 80333 München, Germany.*
[3] *Astrophysikalisches Institut Potsdam, An der Sternwarte 16, 14482 Potsdam, Germany.*
[4] *Astronomy Department, New Mexico State University, Dept. 4500, Las Cruces, NM 88003, United States.*
[⋆] *email jensen@mpa-garching.mpg.de*
[†] *email sgottloeber@aip.de*
[‡] *email aklypin@nmsu.edu*
[§] *email akravtso@nmsu.edu*

Version of 22 June 1999.

ABSTRACT

We use a high–resolution dissipationless simulation to study the evolution of the dark matter and halo distributions in a spatially flat cosmological model dominated by a cosmological constant Λ and cold dark matter (ΛCDM). In order to quantify the evolution of structure, we calculate the Minkowski functionals of the halos and the dark matter component at various redshifts. A comparison of Minkowski functionals and the more standard correlation function analysis shows that the Minkowski functionals contain information about correlation functions of arbitrary order. While little evolution of the Minkowski functionals of halos between $z = 4$ and $z = 0$ is observed, we find that the Minkowski functionals of the dark matter evolve rapidly with time. The difference of the Minkowski functionals of halos and dark matter can be interpreted as a scale dependent bias. This implies that scale–dependent bias is a property of not only the two-point halo correlation function, but also of correlation functions of higher order.

Key words: Methods: statistical; Galaxies: general; Cosmology: theory; dark matter; large–scale structure of Universe.

1 INTRODUCTION

It is generally believed that dark matter (DM) constitutes a large fraction of the mass in the Universe. Therefore, it significantly affects both the process of galaxy formation, and the large–scale distribution of galaxies. The gravitational domination of DM on the scale of the galactic virial radius implies that collisionless simulations can be used to study the formation of the DM halos of galaxies.

The standard flat cosmological scenarios with cold dark matter alone cannot explain the structure formation both on small and very large scales. Recently, scenarios with a nonzero vacuum energy, quantified by the cosmological constant Λ, have been proved to be very successful in describing most of the observational data at both low and high redshifts. Here we study the evolution of the dark matter and halo distributions in a spatially flat cosmological model dominated by the cosmological constant and cold dark matter, ΛCDM.

In order to assess the properties of the dark matter or halo distribution, a variety of statistical methods have been developed. The hierarchy of correlation functions, counts–in–cells or the power spectrum are examples of low–order statistics. While this may be sufficient to characterize the large–scale structure of the Universe, gravitational clustering quickly leads into the nonlinear regime where strongly non–Gaussian structures evolve. More information can then be expected from measures that provide a handle on the global morphology of the large–scale structure. One example of such measures are the Minkowski functionals.

Minkowski functionals have been introduced into cosmology by Mecke et al. (1994). They provide a geometrical and topological description of a point distribution (for a detailed introduction, see Schmalzing et al. 1996). Recently Minkowski functionals have been applied to clusters of galaxies (Kerscher et al. 1997), IRAS galaxies (Kerscher et al. 1998), and anisotropy maps of the cosmic microwave background (Winitzki & Kosowsky 1997; Schmalzing & Górski 1998; Novikov et al. 1998).

Our article is organized as follows. In section 2 we summarize the properties of our ΛCDM simulation, while in section 3 we briefly introduce the method of Minkowski functional analysis. In the following section 4 we apply Minkowski functionals to describe the distribution of dark matter particles and halos. Finally, in section 5 we summarize obtained results and draw our conclusions.

2 THE SIMULATION

We investigate a spatially flat model with a cosmological constant (ΛCDM with $\Omega_0 = 0.3$, $\Omega_\Lambda = 0.7$, $\sigma_8 = 1.0$, and $h = 0.7$). These parameters allow for a power spectrum normalization in accord with both the four year *COBE* DMR observations (Bunn & White 1997) and the observed abundance of galaxy clusters (Viana & Liddle 1996). The age of the universe in this model is ≈ 13.5 Gyrs.

In order to study the statistical properties of halos in a cosmological environment, the simulation box should be sufficiently large; we use a cube of $60h^{-1}$Mpc side length. On the other hand, to assure halo survival in clusters, the force resolution should be $\lesssim 1 - 3h^{-1}$kpc and the mass resolution should be $\lesssim 10^9 h^{-1} M_\odot$ (Moore et al. 1996; Klypin et al. 1999). Our simulations were done using the Adaptive Refinement Tree (ART) code (Kravtsov et al. 1997) with a dynamical range of 32,000 in high density regions. The simulation followed evolution of 256^3 cold dark matter particles, which give particle mass of $1.1 \times 10^9 h^{-1} M_\odot$. The mass resolution is therefore sufficient to identify galaxy–size halos of mass $M \gtrsim 5 - 10 \times 10^{10} h^{-1} M_\odot$.

Identification of halos in dense environments and reconstruction of their evolution is a challenge. A variety of situations that are frequently found in the real Universe are difficult to identify in simulations. Typically, problems arise if a small satellite is bound to a larger galaxy; famous examples are the M51 system, or the LMC and the Milky Way. Cases when many small gravitationally self–bound halos are moving within a large region of virial overdensity, such as clusters and groups of galaxies, can also cause trouble. We have developed two algorithms to deal with such situations, namely the hierarchical friends-of-friends (HFOF) procedure and the bound density maxima (BDM) algorithm (Klypin et al. 1999). Both yield consistent results, i.e. they basically identify the same halos in a DM simulation.

In this study, we use the BDM algorithm to construct halo catalogs at different redshifts. The main idea of the algorithm is to find positions of local maxima in the density field smoothed on a certain scale and to apply physically motivated criteria to test whether the identified site corresponds to a gravitationally bound halo. The density maxima are found iteratively for a series of smoothing scales, the smallest scale being close to the peak resolution of the simulation. To test whether a density maximum corresponds to a real halo, we construct density and velocity dispersion profiles centered on the maximum and iteratively remove unbound particles. This procedure eliminates unbound halos from the catalog, while also cleaning bound halos off some high-velocity background particles. The detailed description of the BDM algorithm is given in (Klypin et al. 1999) and in Colín et al. (1999). The BDM code is available from authors upon request.

Halos are usually characterized by their virial mass. Unfortunately, it is difficult to obtain a meaningful definition of this quantity for halos inside larger halos, so we avoid the problem by determining the maximum circular velocity $v_{\rm circ}$ of each halo. The circular velocity is defined as the maximum of $\sqrt{GM(<R)/R}$, where $M(<R)$ denotes the mass contained inside a sphere of radius R around the halo center, and G is the gravitational constant. $v_{\rm circ}$ is more useful both observationally and numerically. Moreover, it can be measured more easily and more accurately than mass. For isolated halos the maximum circular velocity and the virial radius are, of course, directly related and are therefore equivalent.

The output of the halo finding algorithm is primarily determined by the assumed lower mass threshold and also depends weakly on the assumed maximum halo radius. With the threshold of $10^{10} h^{-1} M_\odot$ (10 particles) at $z = 0$ the algorithm identifies about 17,000 halos in our simulation. In order to conduct a study of halo statistics one needs a complete halo sample that is not affected by the numerical details of the halo finding procedure. We have tested the completeness of the halo samples with the differential velocity functions (Gottlöber et al. 1998). Depending on redshift one can define a threshold of the circular velocities so that for circular velocities larger than this threshold the halo samples do not depend on the numerical parameters of the halo finder. It has been verified that at $z = 0$ the sample is complete for all halos with $v_{\rm circ} \gtrsim 85$km/s, while for $z = 1$ completeness is achieved only with $v_{\rm circ} \gtrsim 100$km/s.

3 MINKOWSKI FUNCTIONALS

Let us consider an object in three–dimensional Euclidean space. Its morphology can be characterized by the four Minkowski functionals, namely the volume V, the surface area A, the integral mean curvature H, and the Euler characteristic χ. Hadwiger (1957) has shown that the Minkowski functionals supply a complete and unique description of the global morphology. As geometrical characteristics of structure, the Minkowski functionals combine both the advantage of a intuitive geometrical interpretation and the advantage of delivering a quantitative measure.

In the following, we look upon the distribution of the dark matter particles and the halos as realizations of point processes. To investigate the distribution of these points we decorate each of them with a ball of radius r. Starting from the trivial situation at $r = 0$, where all points are isolated from each other, we increase r, thereby creating connections between neighboring balls. This procedure results in a complex pattern of intersecting balls the properties of which can be studied using Minkowski functionals. To be precise, we calculate for a set of points $\{\mathbf{x}_j\}$ decorated by balls B of radius r the Minkowski functionals $V_\mu\left(\bigcup_j B_{\mathbf{x}_j}\right)$ of the union set of all balls. Varying the radius introduces a diagnostic parameter into our investigation. Since the set of points is generated by a reasonably well–behaved point process (see Weil 1983 for a rigorous discussion of requirements), we can define an ensemble average of the Minkowski functionals per unit volume. We call these quantities v_μ.

Like other morphological estimators, the Minkowski functionals of a point sample depend on its number density. In the case of a Poisson process one may derive scaling relations with the number density and radius using the analytical results of (Mecke & Wagner 1991) and the homogeneity property of the Minkowski functionals. For general distributions, however, scaling relations are not readily available since the scaling properties depend, even without correlations, on the dimensionality of the support of the point process. This is why we always take care to select the same number of points from our samples before we calculate the Minkowski functionals. However the total number of halos above a certain minimum circular velocity changes with redshift due to merging. Therefore, we proceed as follows: We assume a threshold of 111km/s for the circular velocity $v_{\rm circ}$, and find 5575, 9644, 5869 halos at redshifts 4, 1, and 0, respectively. From these halos we randomly select at each moment 5000 halos, and compute their Minkowski functionals. We do this several times with different random sets to derive a scatter. To compare the distribution of halos with that of dark matter we also select 5000 dark matter particles at random.

All the point samples we study live in cubic boxes with periodic boundary conditions. Hence correction of edge effects as performed, for example, by Schmalzing et al. (1996) in the analysis of real catalogues, is not an issue here. The numerical computation of the Minkowski functionals is performed using an implementation of the partition formula derived by Federer (1959). The formula provides a generalized concept of surface integration, suitable for taking into account the corners and edges encountered in our union set of balls (for a detailed description, see Mecke et al. 1994). The present implementation offers the advantages of scaling linearly with the number of points, and requiring only moderate computational resources; a sample of 5000 points can be fully analyzed in about one hour on an average workstation. Together with a parallelized version, the source of the code used in this work is available from the authors upon request.

4 ANALYSIS

4.1 Evolution of two-point correlation function and Minkowski functionals

Recently, the evolution of clustering of dark matter halos has been investigated for several cosmological models using numerical dissipationless simulations (Brainerd & Villumsen 1994; Bagla 1998; Colín et al. 1999; Kravtsov & Klypin 1999; Ma 1999), simulations that include both dissipationless dark matter and dissipative baryonic components (Katz et al. 1999; Blanton et al. 1998; Blanton et al. 1999; Cen & Ostriker 1999; Jenkins et al. 1998), and "hybrid" studies in which dissipationless simulations are complemented with a semi-analytical model of galaxy formation (Roukema et al. 1997; Kauffmann et al. 1999a; Kauffmann et al. 1999b; Diaferio et al. 1999; Baugh et al. 1999; Benson et al. 1999; Kolatt et al. 1999). All of these studies, though very diverse in their methods, qualitatively agree on one important result:

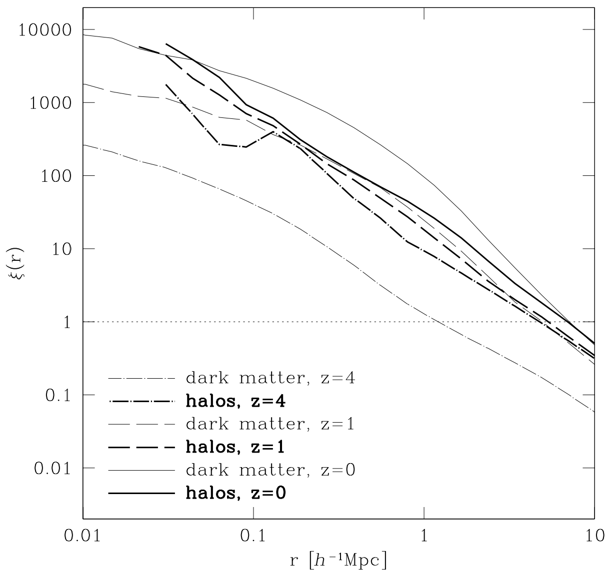

Figure 1. Correlation functions of the halo samples ($v_{\rm circ}$ > 111km/s) and the dark matter distributions at $z = 0$, 1, 4.

bias is expected to be non–linear, to depend on the properties of the DM halos and the galaxies they host, and to be a (generally non–monotonic) function of cosmic time.

In particular, Colín et al. (1999) discuss the evolution of the real space two-point correlation function in different cosmological models. They find that in all models and at all epochs, the correlation function of halos can be reasonably approximated by a power–law. In Figure 1 we compare the correlation function of the dark matter particles in real space with the correlation function of halos with circular velocities $v_{\rm circ}$ > 111km/s. In agreement with previous studies, we see almost no evolution of the halo correlation function between redshifts 4 and 0, whereas by comparison the correlation function of the dark matter particles increases with time.

The four Minkowski functionals for halos and dark matter particles at various epochs are shown in Figures 2 and 3, respectively. The scatter between different subsamples is marginally larger than the line width, so for clarity we only plot the mean values. One should keep in mind that due to the density dependence of the Minkowski functionals the diagnostic parameter "radius" cannot be directly associated with a scale. Instead, the general features described below occur within the radius range between zero and a few times the average distance for any point distribution studied. It is the location and relative strength of these features that accounts for the discriminative power of the Minkowski functionals. Quantitative measurements may be possible using reference distributions; the simplest such case is the Poisson process displayed in all Figures.

The zeroth Minkowski functional is nothing but one less the void probability function (VPF), which is defined as the probability of finding no objects within randomly placed

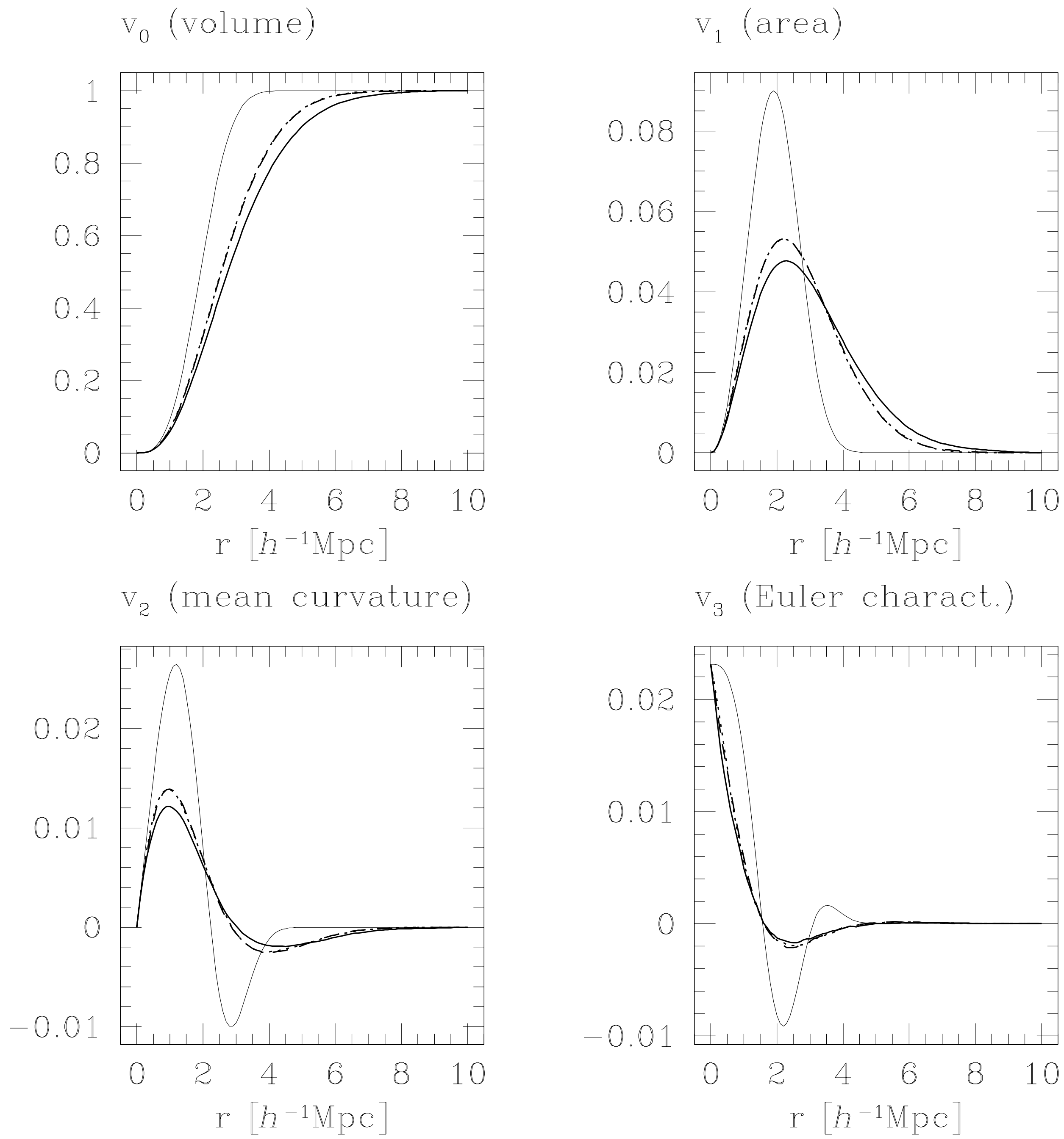

Figure 2. Minkowski functionals of the halo samples ($v_{\rm circ} > 111$km/s) samples at $z = 0$ (solid), $z = 1$ (dashed) and $z = 4$ (dotted). Note that the results for $z = 1$ and $z = 4$ coincide almost everywhere, so the lines appear dash–dotted. As a standard of reference, we show the analytically known values for a Poisson process of the same intensity (thin solid line).

balls (for a recent study of the VPF of halos, see Ghigna et al. 1996). Voids are successively filled as the radius of balls increases, so the v_0 increases monotonically approaching a value of one at complete filling of the whole simulation box. The first and second Minkowski functionals are related to the surface content and the integrated mean curvature of the body, and have rarely been applied in cosmology. Both quantities start from a value of zero at zero radius, and increase to a maximum value. While the area only decreases from that point, as the union set becomes more connected, the integrated mean curvature shows a turnover from positive to negative values, indicating a change from convex

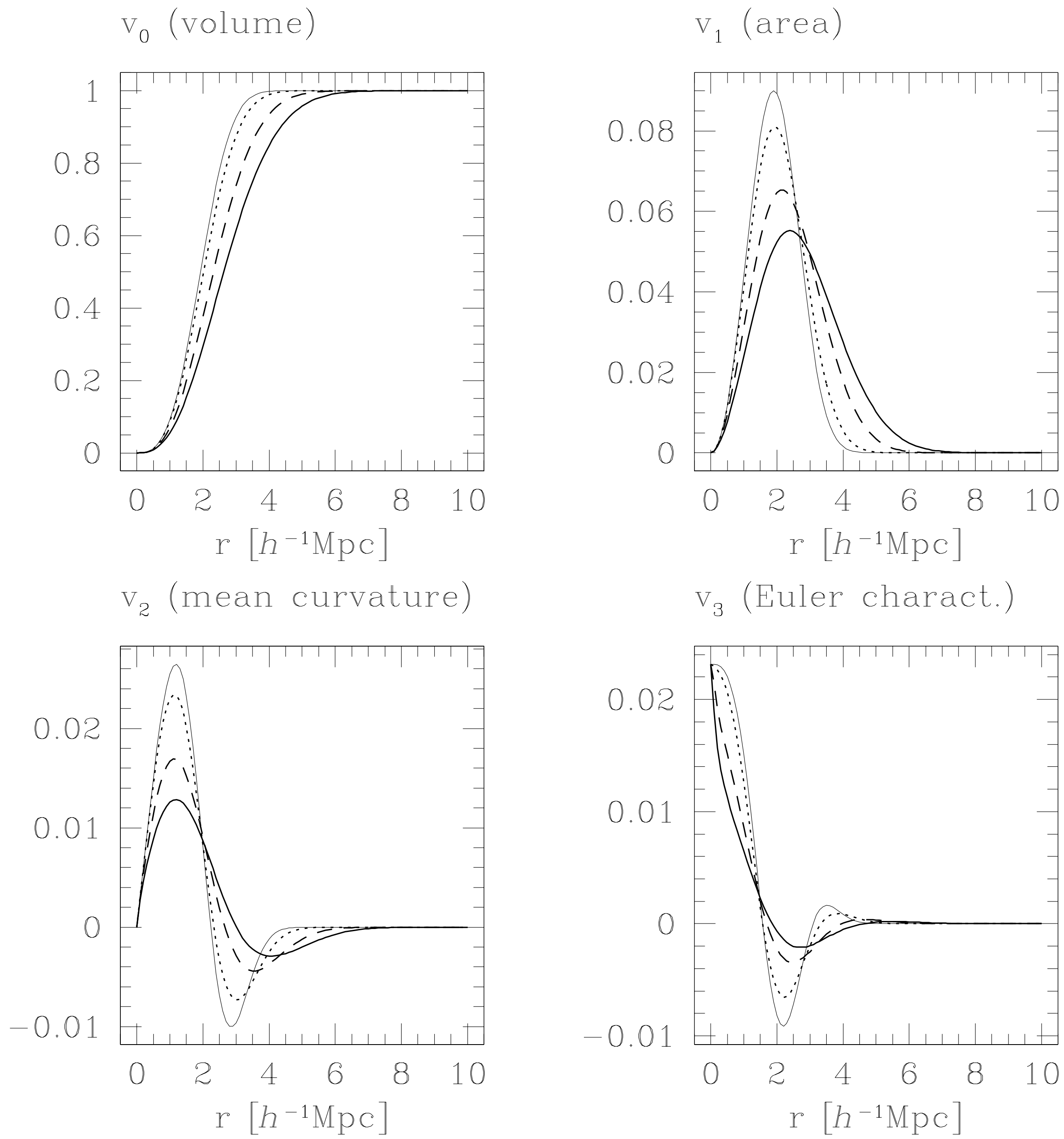

Figure 3. Minkowski functionals of the dark matter distribution at $z = 0$ (solid), $z = 1$ (dashed) and $z = 4$ (dotted). As in Figure 2, we include a Poisson process(thin solid line).

to concave structures. The third Minkowski functional, the Euler characteristic v_3, is a purely topological quantity and counts the number of components less the number of tunnels in a structure. At small radii, all balls are isolated from each other and v_3 is simply equal to the number density of points. As connections are established between closely neighboring points, the Euler characteristic decreases and eventually falls below zero, when an intricate network of tunnels has formed in the union set. A second maximum is reached at an already fairly large filling factor, when the union set mainly contains isolated cavities, which count as components and each contribute +1 to the Euler characteristic. Eventually the whole box is filled and v_3 becomes zero. Note that the Euler characteristic v_3 is connected to the genus g via $g = 1 - 2v_3$. The genus has been already widely discussed in the cosmological context using density fields constructed by fixed–width smoothing the particle distribution (Gott III et al. 1986). The result then depends on both the smoothing scale and the density threshold which has been used for the construction of the body.

In Figure 2 we show the Minkowski functionals of 5000 randomly selected halos at redshifts $z = 4$, 1, and 0. We do not show the scatter resulting from different selection, since the standard deviation is of the order of the line width. Only little evolution of the clustering of halos can be seen. In particular, the Minkowski functionals at $z = 4$ and $z = 1$ coincide, while the number of halos with $v_{\rm circ} > 111$km/s increases in this time interval by almost a factor of two. If one calculates the Minkowski functionals of all halos above that threshold of the circular velocity one would see weaker clustering at $z = 1$ than at $z = 4$. This demonstrates the importance of selecting the same number of objects for the comparison of Minkowski functionals.

Already at $z = 4$ the Minkowski functionals of halos are markedly different from a Poisson process. We interpret the evolution of the Minkowski functionals in the long time interval between $z = 1$ and $z = 0$ as nonlinear clustering on small scales (see Kravtsov & Klypin 1999 for a detailed discussion). The halos tend to move towards existing clusters of halos, hence the void probability function increases on all scales, and both surface and mean integral curvature decrease on small scales.

It is remarkable that the Euler characteristic of the halo distribution hardly changes with time. The absence of the positive maximum of v_3 at any time and any radius in the halo distribution can be interpreted as the signature of a network of filaments or sheets, which leave only few cavities in the almost filled union set. Furthermore, the sharp drop of the Euler characteristic at small radii points towards strong clustering on small scales. These features reveal the presence of a network of filamentary structures spanning the whole simulation box. We are confident that our result is only weakly influenced by the comparatively small box size of $60h^{-1}$Mpc. After all, two points in the set can only influence each other's contribution to the Minkowski functionals if they are less than twice the radius apart. However, complete filling occurs below $10h^{-1}$Mpc, i.e. almost an order of magnitude below the box size.

In contrast to the modest evolution seen in the halo distribution, the clustering of dark matter shown in Figure 3 evolves considerably with time. The present day clustering of DM appears to be as strong as that of the $z = 0$ halo sample. At $z = 4$, however, the DM clustering properties still resemble those of the Poisson process. The modest differences from a purely random distribution reflect that most of the particles are still contained in the field, and only a minority has formed structures. Even if the sampling density is increased, this effect persists.

Finally, let us compare the Minkowski functionals of the DM and halo distributions. The DM distribution evolves continuously towards higher clustering as one has seen already from the analysis of the evolution of the correlation function and the power spectrum. At early epochs the Minkowski functionals indicate a much stronger clustering of the halos than

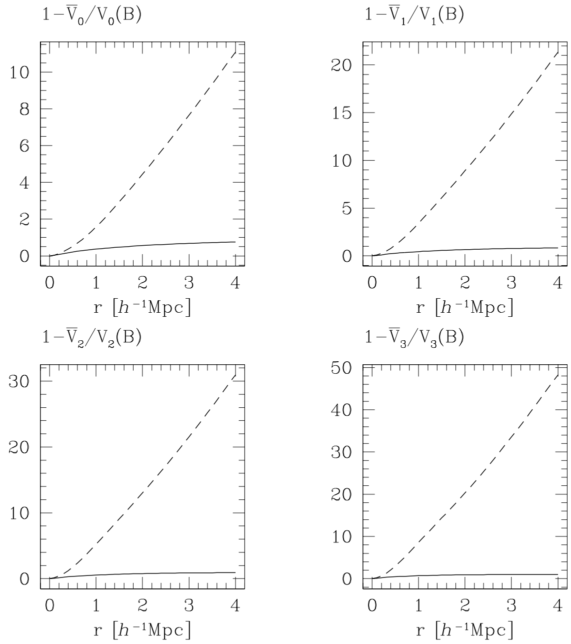

Figure 4. For halos at $z = 0$ we compare the asymptotic series from Eq. (A12) (solid line) to its truncation after the first non–trivial term, which contains a convolution of the two point correlation function. The dashed line is obtained using the halo correlation function of Fig. (1).

μ	$V_\mu(B)$	$\frac{V_\mu(B \cap B_{\mathbf{x}})}{V_\mu(B)}$
0	$4\pi r^3/3$	$(1-d)^2(1-d/2)$
1	$2\pi r^2/3$	$1-d$
2	$4r/3$	$1-d+(\sqrt{1-d^2}/2)\arcsin d$
3	1	1

Table 1. Minkowski functionals of a single ball B of radius r and of an intersection $B \cap B_{\mathbf{x}}$ of two balls separated by a distance $x = 2rd$ $(0 \le d \le 1)$.

of DM, but there is only a little difference in the morphological properties of halo and DM distribution at $z = 0$ (cf. Sect. 4.3).

4.2 Comparison to Correlation Function Analysis

In theory, Minkowski functionals contain information about correlation functions of arbitrary order. However, it is not clear a priori that this actually results in enhanced information compared to the standard correlation function analysis. Although the analysis of the previous section revealed a wealth of information on the evolution of clustering in our simulation, it seems that qualitatively the same information could have been deduced from the correlation function alone. In Appendix A we establish an analytical connection between the hierarchy of correlation functions and the

Minkowski functionals, and use this relation to conduct a direct comparison.

The Minkowski functionals per unit volume, v_μ, of a Poisson process with intensity ρ are given by

$$v_0 = 1 - \mathrm{e}^{-\rho V_0(B)}$$
$$v_1 = \mathrm{e}^{-\rho V_0(B)} \rho V_1(B)$$
$$v_2 = \mathrm{e}^{-\rho V_0(B)} \left(\rho V_2(B) - \frac{3\pi}{8}\rho^2 V_1(B)^2\right)$$
$$v_3 = \mathrm{e}^{-\rho V_0(B)} \left(\rho V_3(B) - \frac{9}{2}\rho^2 V_1(B) V_2(B) + \frac{9\pi}{16}\rho^3 V_1(B)^3\right) \tag{1}$$

where $V_\mu(B)$ is the μth Minkowski functional of a ball B of radius r. As shown in Appendix A this formula can be generalized for arbitrary point processes, if the $V_\mu(B)$ are replaced by a series $\overline{V}_\mu$ containing the complete hierarchy of correlation functions. Truncating Equation (A12) after the first two terms we have

$$\overline{V}_\mu = V_\mu(B) - \frac{\rho}{2}\int \mathrm{d}^3x\,\xi(x) V_\mu(B \cap B_x) \pm \ldots \tag{2}$$

In Table 1 we summarize the Minkowski functionals $V_\mu(B)$ of a single ball B of radius r and of an intersection $B \cap B_{\mathbf{x}}$ of two balls separated by a distance $x = 2rd$ $(0 \leq d \leq 1)$. Note, that all Minkowski functionals of the empty intersection $x > 2r$ become zero.

In Figure 4 we present the asymptotic series $\overline{V}_\mu$ of the halo distribution at $z = 0$ (solid line). We compare the full asymptotic series obtained by inverting Eq.(A11) with its truncation after the first non–trivial term (dashed line) according to Eq. (2). Here we use the halo two-point correlation function at $z = 0$ determined from the simulation as presented in Fig. 1. Obviously, the leading terms do not even vaguely approximate the full series from Equation (2).

Integrating Eq. (2) with a standard power-law correlation function $\xi(x) = x^{-\gamma}$ we obtain the scaling behavior

$$1 - \overline{V}_\mu / V_\mu(B) \propto r^{3-\gamma} \tag{3}$$

for the truncated series. For clarity, we have not included these curves in Fig. 4, but with $\gamma = 1.7$, a reasonable fit to the curve calculated from the numerically determined correlation function can be obtained. This confirms that the Minkowski functionals reveal information beyond the correlation function analysis, and sharply discriminate between the halo distribution of our model and a purely Gaussian process with the same second–order characteristics. Since they reveal clustering properties of a totally different quality, Minkowski functionals are an ideal complement to more standard methods of large–scale structure analysis.

4.3 Bias

The comparison of Minkowski functionals on its own provides a qualitative understanding of the clustering properties of matter in the model. In this section we compare directly the clustering properties of DM and halos at $z = 0$. It is well known that the distribution of halos is different from the DM distribution. The relationship between these two distributions is called bias. Considering the correlation

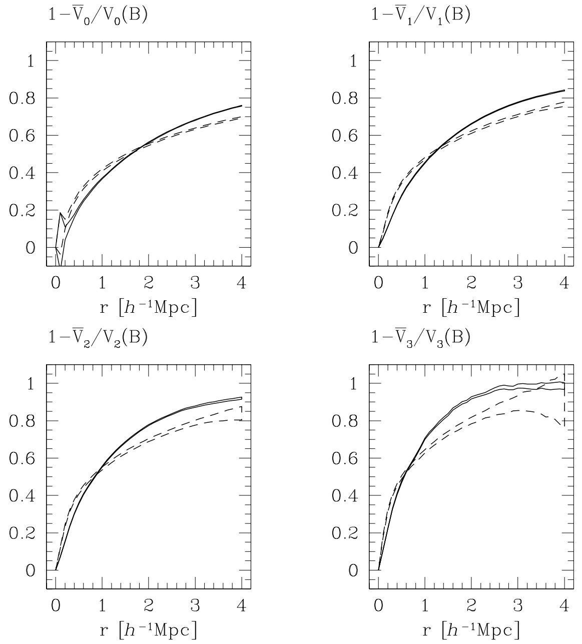

Figure 5. In these plots we compare the ratios $1 - \overline{V}_\mu / V_\mu(B)$ for halos (solid lines) and dark matter particles (dashed lines) at redshift $z = 0$. The areas indicate the standard deviation between different subsamples of the point distribution.

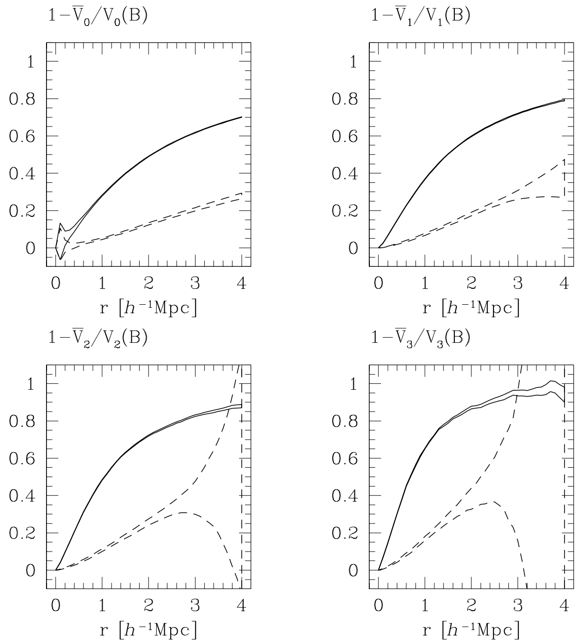

Figure 6. As in Figure 5, these plots show the ratios $1 - \overline{V}_\mu / V_\mu(B)$ for halos (solid lines) and dark matter particles (dashed lines), but at redshift $z = 4$. Again, the areas display the scatter between subsamples of 5000 points taken from the whole particle distribution.

functions of halos and DM the ratio between both can be interpreted as scale–dependent bias (Fig. 1).

This scale–dependent bias is a generic prediction of hierarchical models of structure formation (Colín et al. 1999). The bias is also time-dependent: it decreases from an initially high value at $z \sim 3-7$ to a considerably smaller value (which can be even less than one) at present. Qualitatively, the same behavior has been found in the power spectrum both in real space (Kravtsov & Klypin 1999) and in redshift space (Gottlöber et al. 1998). Since power spectrum and correlation function are the Fourier pairs, a bias in one of them leads to a bias in the other. Obviously, any scale dependence will be different in coordinate and k space.

In Figures 5 and 6 we compare the functions $1-\overline{V}_\mu/V_\mu(B)$ for the dark matter and halos. Our analysis indicates that these functions (the solid lines in Figure 4) are much more suitable for comparison than the Minkowski functionals themselves. For example, $1-\overline{V}_\mu/V_\mu(B)=0$ is expected in case of a Poisson process. The figure shows these quantities for halos (solid lines) and dark matter particles (dashed lines). At $z=0$, bias is a lot weaker than at $z=4$. For small radii, an anti–bias is observed, meaning that halos appear less clustered than dark matter particles. This does not occur at higher redshifts, where halos cluster stronger than dark matter particles at all radii. Although the radii for which the halo and DM curves coincide are different for the four functionals and different from the radius where the correlation functions of halos and DM coincide, the qualitative appearance of all Minkowski functionals is similar; this reflects the fact that all $\overline{V}_\mu$ depend on the hierarchy of correlation functions in a very similar way through Equation (A12).

The two solid and dashed lines in each of the panels indicate the scatter which we have estimated from the statistics for different random selections of 5000 objects. At large radii, uncertainties increase because the Boolean grain model already fills a considerable portion of the whole space, and small fluctuations in the pattern have strong effects on its morphology. This effect is expected to be strongest for structures that eventually form cavities in an almost solid body. In fact the dark matter distribution shows much more scatter at larger radii, compared to the fairly filamentary halo distribution. While the scatter described so far is an intrinsic feature of the point process, the very large error for the volume functionals at small radii is due to the Monte Carlo integration used for the numerical evaluation; by increasing the number of Monte Carlo points, it can be somewhat reduced but not fully eliminated.

It is interesting to discuss the anti-bias of halo distribution observed in all of the Minkowski functionals at $z=0$. Note that our halo finder algorithm identifies both isolated halos and halos located within virial radii of other halos (satellites; see Colín et al. 1999 for details). Therefore, the small–scale anti-bias is not caused by the characteristic size of the halos and their mutual exclusion. Note, for example, that there is no indication of similar anti-bias at $z=4$. Rather, as was shown by Kravtsov & Klypin (1999), the anti–bias is most likely due to dynamical friction and (to a lesser degree) to the tidal stripping in the high–density environments of groups and clusters. Indeed, the dynamical friction results in mergers of satellite halos with the central cluster halo and thereby reduces the ratio of halo overdensity to the ever–growing overdensity of dark matter. We refer the reader to Kravtsov & Klypin (1999) for an extended discussion and tests of the origin and evolution of halo anti-bias. Here we note that if the anti–bias is indeed due to the dynamical processes affecting galaxy evolution in groups and clusters, studies of higher–order small–scale galaxy clustering and its dependence on morphology may prove to be useful and independent probes of galaxy evolution in dense environments.

5 SUMMARY AND CONCLUSIONS

We have used a high–resolution dissipationless simulation of the formation of dark matter halos in a flat cosmological model dominated by the cosmological constant and cold dark matter. In the $60h^{-1}$ Mpc simulation box we have identified 5575, 9644, and 5869 halos of maximum circular velocity $v_{\rm circ} > 111$km/s at redshifts 4, 1, and 0, respectively.

At each of these epochs we have calculated the Minkowski functionals for bodies constructed as a Boolean grain model of 5000 randomly selected halos and 5000 randomly selected dark matter particles, respectively. The Minkowski functionals focus on global features of three–dimensional bodies, and provide a unifying frame for the analysis of cosmic structures which comprises the void probability function as well as the genus statistics. Minkowski functionals do not replace but complement such traditional tools as the two–point correlation function, since they reveal clustering properties of higher-order.

We found almost no evolution of the Minkowski functionals of halos between $z=4$ and $z=1$ and little evolution between $z=1$ and $z=0$. The rather small differences at various epochs are mainly due to evolution of nonlinear clustering on small scales. Already at $z=4$ the Minkowski functionals of halos are markedly different from a Poisson process. We can deduce that from the beginning, luminous matter quickly forms complicated structure on large scales, which may be interpreted as a network of sheets and filaments.

On the other hand, the clustering of dark matter evolves considerably with time. At $z=4$ the clustering properties of DM mostly resemble those of the Poisson process, with only minor deviations. At the present epoch, the clustering is as strong as for the halo sample, although the morphology of the dark matter distribution differs from the structure formed by the halos.

The difference of the Minkowski functionals of halos and dark matter can be interpreted as a scale dependent bias which is qualitatively similar but quantitatively different for each of the Minkowski functionals. The evolution of halo bias in the linear and mildly nonlinear regimes results from an interplay between halo formation and merging rates in different regions and in the field. Both rates are non-monotonic functions of time, but their combined effect is decrease of the initially high *statistical* bias during the course of the evolution. In the non-linear regime, the halo bias evolution may be also affected by the dynamical processes inside clusters and groups (Kravtsov & Klypin 1999).

We have demonstrated in this paper that the Minkowski functionals contain information about the correlation functions of arbitrary order. Therefore, our results imply that the scale-dependent bias is a property of not only the two-point halo correlation function, but also of the correlation functions of higher order. This, in turn, means that there are morphological differences between distributions of halos and matter at both small and large scales. In particular, at early epochs the halos are already strongly clustered and their distribution shows distinct features of a network. The dark matter distribution at the same epochs is still weakly clustered and is close to the Poisson distribution. At the present epoch the halo distribution appears less clustered on small scales, while it remains more filamentary on large scales than the distribution of matter. Whether the measured Minkowski functionals indicate the abundance of filaments or sheets or both in the network is currently an open question. Although the very steep initial rise of the curves in Figure 5 would favor a filamentary distribution, sheet–like structures are not ruled out either. Quantitative measurements of planarity and filamentarity will be the subject of a follow–up article.

ACKNOWLEDGMENTS

This work was funded by grants from the NSF and NASA to NMSU. We acknowledge support by the NATO grant CRG 972148. SG acknowledges support from the Deutsche Akademie der Naturforscher Leopoldina with means of the Bundesministerium für Bildung und Forschung grant LPD 1996. JS wishes to thank the AIP for hospitality during a stay where parts of this work were prepared. The simulation presented here was performed at the National Center for Supercomputer Applications (NCSA, Urbana-Champaign, Illinois) and on the Origin2000 computer at the Naval Research Laboratory.

Please note that the code used for this analysis is publicly available and can be obtained by sending email to `jensen@mpa-garching.mpg.de`.

References

Bagla, J., Mon. Not. Roy. Astron. Soc. **299** (1998), 417–424.

Balian, R. & Schaeffer, R., Astron. Astrophys. **220** (1989), 1–29.

Balian, R. & Schaeffer, R., Astron. Astrophys. **226** (1989), 373–414.

Baugh, C., Benson, A., Cole, S., Frenk, C. S., & Lacey, C. G., Mon. Not. Roy. Astron. Soc. **305** (1999), L21–L25.

Benson, A., Cole, S., Frenk, C. S., Baugh, C., & Lacey, C. G., Mon. Not. Roy. Astron. Soc. (1999), submitted, astro-ph/9903343.

Blanton, M., Cen, R., Ostriker, J. P., & Strauss, M. A., Ap. J. (1998), submitted, astro-ph/9807029.

Blanton, M., Cen, R., Ostriker, J. P., Strauss, M. A., & Tegmark, M., Ap. J. (1999), submitted, astro-ph/9903165.

Blaschke, W., *Integralgeometrie. Erstes Heft*, Bernd G. Teubner, Leipzig, Berlin, 1936.

Brainerd, T. G. & Villumsen, J., Ap. J. **436** (1994), 528–541.

Bunn, E. F. & White, M., Ap. J. **480** (1997), 6–21.

Cen, R. & Ostriker, J. P., Ap. J. (1999), submitted, astro-ph/9809370.

Chern, S.-S. & Yien, C.-T., Bollettino della Unione Matematica Italiana **2** (1940), 434–437.

Coles, P. & Jones, B., Mon. Not. Roy. Astron. Soc. **248** (1991), 1–13.

Colín, P., Klypin, A. A., Kravtsov, A. V., & Khokhlov, A., Ap. J. (1999), to appear in September 20 issue.

Diaferio, A., Kauffmann, G., Colberg, J. M., & White, S. D., Mon. Not. Roy. Astron. Soc. (1999), in press, astro-ph/9812009.

Federer, H., Trans. Amer. Math. Soc. **93** (1959), 418–491.

Ghigna, S., Bonometto, S. A., Retzlaff, J., Gottlöber, S., & Murante, G., Ap. J. **469** (1996), 40–47.

Gott III, J. R., Melott, A. L., & Dickinson, M., Ap. J. **306** (1986), 341–357.

Gottlöber, S., Klypin, A. A., Kravtsov, A. V., & Khokhlov, A., in: *Observational Cosmology: The Development of Galaxy Systems* (Congresso Sesto), PASP Conference Proceedings Series, 1998, astro-ph/9810445.

Hadwiger, H., *Vorlesungen über Inhalt, Oberfläche und Isoperimetrie*, Springer Verlag, Berlin, 1957.

Hadwiger, H., Mh. Math. **79** (1975), 213–221.

Jenkins, A., Frenk, C. S., Pearce, F. R., Thomas, P. A., Colberg, J. M., White, S. D. M., Couchman, H. M. P., Peacock, J. A., Efstathiou, G., & Nelson, A. H., Ap. J. **499** (1998), 20–40.

Katz, N., Hernquist, L., & Weinberg, D. H., Ap. J. (1999), submitted, astro-ph/9806257.

Kauffmann, G., Colberg, J. M., Diaferio, A., & White, S. D., Mon. Not. Roy. Astron. Soc. **303** (1999), 188–206.

Kauffmann, G., Colberg, J. M., Diaferio, A., & White, S. D., Mon. Not. Roy. Astron. Soc. (1999), in press, astro-ph/9809168.

Kellerer, H., Z. Wahrscheinlichkeitstheorie verw. Gebiete **67** (1984), 63–84.

Kerscher, M., Schmalzing, J., Retzlaff, J., Borgani, S., Buchert, T., Gottlöber, S., Müller, V., Plionis, M., & Wagner, H., Mon. Not. Roy. Astron. Soc. **284** (1997), 73–84.

Kerscher, M., Schmalzing, J., Buchert, T., & Wagner, H., Astron. Astrophys. **333** (1998), 1–12.

Klypin, A. A., Gottlöber, S., Kravtsov, A. V., & Khokhlov, A. M., Ap. J. **516** (1999), 530–551.

Kolatt, T. S., Bullock, J., Somerville, R., Sigad, Y., Jonson, P., Kravtsov, A. V., Klypin, A. A., Primack, J. R., & Dekel, A., Science (1999), submitted.

Kravtsov, A. V. & Klypin, A. A., Ap. J. (1999), to appear in August 1 issue.

Kravtsov, A. V., Klypin, A. A., & Khokhlov, A. M., Ap. J. Suppl. **111** (1997), 73–94.

Ma, C.-P., Ap. J. **510** (1999), 32–41.

Mecke, K. R. & Wagner, H., J. Stat. Phys. **64** (1991), 843.

Mecke, K. R., Buchert, T., & Wagner, H., Astron. Astrophys. **288** (1994), 697–704.

Moore, B., Katz, N., & Lake, G., Ap. J. **457** (1996), 455–459.

Novikov, D., Feldman, H. A., & Shandarin, S. F., Ap. J. (1998), submitted, astro-ph/9809238.

Roukema, B., Peterson, B., Quinn, P., & Rocca-Volmerange, B., Mon. Not. Roy. Astron. Soc. **292** (1997), 835–852.

Schmalzing, J. & Górski, K. M., Mon. Not. Roy. Astron. Soc. **297** (1998), 355–365.

Schmalzing, J., Kerscher, M., & Buchert, T., in: *Proceedings of the international school of physics Enrico Fermi. Course CXXXII: Dark matter in the Universe* (Varenna sul Lago di Como) (Bonometto, S., Primack, J., & Provenzale, A., eds.), Società Italiana di Fisica, 1996, pp. 281–291.

Viana, P. & Liddle, A., Mon. Not. Roy. Astron. Soc. **281** (1996), 323–332.

Weil, W., in: *Convexity and its applications* (Gruber, P. M. & Wills, J. M., eds.), Birkhäuser, Basel, 1983, pp. 360–412.
White, S. D. M., Mon. Not. Roy. Astron. Soc. **186** (1979), 145–154.
Winitzki, S. & Kosowsky, A., New Astronomy **3** (1997), 75–100.

APPENDIX A: MINKOWSKI FUNCTIONALS EXPRESSED IN TERMS OF CORRELATION FUNCTIONS

It is known that Minkowski functionals contain correlation functions of arbitrary order. Here we aim to establish a precise relation between the average Minkowski functionals v_μ per unit volume in terms of the hierarchy of correlation functions ξ_n of the point process.

In order to cut down on notation we always use a linear combination of Minkowski functionals, the so–called Minkowski polynomial $M(t)$ (Hadwiger 1975; Kellerer 1984). We define

$$M(t;K) = \sum_{\mu=0}^{d} \frac{\alpha_\mu t^\mu}{\mu!} V_\mu(K) \tag{A1}$$

with coefficients[⋆]

$$\alpha_\mu = \frac{\omega_{d-\mu}}{\omega_d}. \tag{A2}$$

Analogously, we construct a polynomial $m(t)$ from the densities v_μ of the Minkowski functionals per unit volume. From now on, we drop the variable t from the polynomial, and only reintroduce it when extracting the individual Minkowski functionals via

$$V_\mu(K) = \frac{1}{\alpha_\mu}\frac{\partial^\mu}{\partial t^\mu} M(t;K). \tag{A3}$$

By taking the ensemble average and applying the additivity relation repeatedly, we obtain the formula given by Mecke et al. (1994),

$$m = 1 - \sum_{n=0}^{\infty} \frac{(-1)^n}{n!} \int \mathrm{d}\tau_n \rho_n\left(\mathbf{x}_1,\ldots,\mathbf{x}_n\right) M\left(B_{\mathbf{x}_1}\cap\ldots\cap B_{\mathbf{x}_n}\right), \tag{A4}$$

with the integration measure defined by

$$\int \mathrm{d}\tau_n = \int_{\mathcal{D}} \mathrm{d}^d x_1 \ldots \mathrm{d}^d x_n. \tag{A5}$$

If the density functions ρ_n were independent of position, the integrals could be performed using the principal kinematic formula by Blaschke (1936) (see also Chern & Yien 1940 for the more general version employed here). Fixing one body A in space, and intersecting with a moving body B, we obtain after integration over all possible positions of B a simple factorization.

$$\int_{\mathcal{D}} \mathrm{d}^d x\, M(A\cap B_{\mathbf{x}}) = M(A)M(B), \tag{A6}$$

where equality holds to order t^d. Unfortunately, straightforward application of the principal kinematic formula to Equation (A4) is impossible in most situations since the density functions are in general position dependent. However, it is possible to use the factorization properties of the density functions into the correlation functions.

Equation (A4) motivates the introduction of a hierarchy of "moments" P_n by weighting the n–point density function with the Minkowski polynomial of n intersecting balls,

$$P_n = \int \mathrm{d}\tau_n \rho_n\left(\mathbf{x}_1,\ldots,\mathbf{x}_n\right) M\left(B_{\mathbf{x}_1}\cap\ldots\cap B_{\mathbf{x}_n}\right). \tag{A7}$$

Writing the density functions ρ_n as sums over all possible partitions into correlation functions ξ_n, and using the principal kinematic formula, it can be shown that the "cumulants" corresponding to the moments P_n are the Ξ_n given by

$$\Xi_n = \int \mathrm{d}\tau_n \xi_n\left(\mathbf{x}_1,\ldots,\mathbf{x}_n\right) M\left(B_{\mathbf{x}_1}\cap\ldots\cap B_{\mathbf{x}_n}\right). \tag{A8}$$

Given a generating functional $P[j]$ for the P_n, a generating functional $\Xi[j]$ for the Ξ_n is obtained through

$$P[j] = \exp\left(\Xi[\rho j]\right). \tag{A9}$$

Setting $j=-1$, we directly arrive at the result

$$m = 1 - \sum_{n=0}^{\infty}\frac{(-1)^n}{n!}P_n = 1 - \exp\left(\sum_{n=0}^{\infty}\frac{(-\rho)^n}{n!}\Xi_n\right). \tag{A10}$$

Recovering the Minkowski functionals from the polynomial via Equation (A3), the relation in $d=3$ dimensions reads

$$\begin{aligned} v_0 &= 1-\exp\left(-\rho\overline{V}_0\right)\\ v_1 &= \exp\left(-\rho\overline{V}_0\right)\rho\overline{V}_1\\ v_2 &= \exp\left(-\rho\overline{V}_0\right)\left(\rho\overline{V}_2 - \frac{3\pi}{8}\rho^2\overline{V}_1^2\right)\\ v_3 &= \exp\left(-\rho\overline{V}_0\right)\left(\rho\overline{V}_3 - \frac{9}{2}\rho^2\overline{V}_1\overline{V}_2 + \frac{9\pi}{16}\rho^3\overline{V}_1^3\right)\end{aligned} \tag{A11}$$

which looks remarkably similar to the result for the Poisson process, except that the bare Minkowski functionals of balls $V_\mu(B)$ are replaced by the quantities

$$\overline{V}_\mu = V_\mu(B) + \sum_{n=1}^{\infty}\frac{(-\rho)^n}{(n+1)!}\int_{\mathcal{D}}\mathrm{d}^d x_1\ldots\mathrm{d}^d x_n\, \xi_{n+1}(0,\mathbf{x}_1,\ldots,\mathbf{x}_n)V_\mu(B\cap B_{\mathbf{x}_1}\cap\ldots\cap B_{\mathbf{x}_n}). \tag{A12}$$

Note that Equation (A12) is a generalization of the result by White (1979) for the void probability function. This shows that all Minkowski functionals depend on the complete hierarchy of correlation functions through an asymptotic series, hence each order n can be expected to contribute significantly to the overall result. In Section 4 this claim is backed by a direct comparison of numerical results.

While it looks promising to push these analytical considerations forward towards a hierarchical model (Balian & Schaeffer 1989a; Balian & Schaeffer 1989b) or a lognormal Cox process (Coles & Jones 1991), we will stop here, since the series to second order is sufficient for our purposes.

⋆ ω_μ denotes the volume of the μ–dimensional unit ball. Some important special values are $\omega_0=1$, $\omega_1=2$, $\omega_2=\pi$, and $\omega_3=\frac{4}{3}\pi$.